High Impedance Surface Electromagnetic Band Gap Metamaterials: Design approach and applications for antenna engineering

Tian Hong Loh
Electromagnetic Technologies Group,
Time, Quantum and Electromagnetics Division,
National Physical Laboratory,
Hampton Road, Teddington, Middlesex TW11 0LW, UK
Email: tian.loh@npl.co.uk

Abstract

This paper presents a theoretical study, design approaches and the applications of mushroom-like High Impedance Surface Electromagnetic Band Gap (HIS-EBG) metamaterials in antenna engineering. The work focuses on techniques for developing HIS-EBG metamaterials that are wideband and compact in size using an electrically tunable approach. A tunable HIS-EBG structure is represented by a novel analytic equivalent transmission line circuit model for surface wave propagation. The analytical and numerical simulations and a parametric study on the effects of patch width, gap width, substrate thickness and substrate permittivity are presented.

Introduction

Important considerations for antenna designers of compact high data rate wireless communications systems are wideband performance and antenna size reduction. However, in many cases, for the size reduction, the main problem is the reduction of ground plane size, given the limited area available on the platforms. Such reduction means an increase in antenna backward radiation even for larger sizes, a normal conducting metal ground plane allows for surface wave propagation, which also contributes to backward radiation via edge diffraction.

In the late 1990s, new forms of artificially fabricated metallo-dielectric electromagnetic structures were invented for radio frequencies and microwaves [1]. Since then, these periodic lattices are have become known as Electromagnetic Band Gap (EBG) structures, which are categorised as a class of metamaterials [2]. These EBG structures exhibit exciting electromagnetic properties such as in-phase reflection and surface wave suppression [3] and thus they have attracted increasing interest in the electromagnetic and antenna community. Their designs have flourished, and a wide variety of materials and geometries have been investigated [4-6].

Among the inventions, an important structure is the mushroom-like High Impedance Surface EBG (HIS-EBG) structure [7], which exhibits high surface impedances for both transverse electric (TE) and transverse magnetic (TM) polarisations and can suppress surface wave propagation at certain frequency ranges. Furthermore, the surface wave band gap property of HIS-EBG helps to increase the antenna gain, minimise backward radiation, and reduce mutual coupling. Hence, they have played an important role in recent developments of new materials for applications in wireless radio communications and antenna engineering. In this paper, we focus on a theoretical study of mushroom-like two-layer HIS-EBG structures, their design approaches and applications to antenna engineering.

Mushroom-like HIS-EBG structure: Design approach and parametric study

As depicted in Figure 1, the unit-cell of a mushroom-like two-layer HIS-EBG structure consists of a square patch, a metallic ground plane, a via connected between the patch and the metallic ground plane, and a square block of substrate. It operates at frequencies where the periodicity is small compare to the operating wavelength of incident waves. In Figure 1, the parameters of the HIS-EBG structure: w, g, D, h, ε_{r_1}, μ_{r_1}, ε_{r_2}, μ_{r_2} and r, are respectively, the width of the patch, the gap width between adjacent patches, the lattice constant, the substrate thickness, the permittivity and permeability of the material surrounding the HIS-EBG, the substrate permittivity, the substrate permeability and the radius of the vertical conducting vias. These parameters can be used to tailor the characteristics of the surface impedance. For example, by applying a texture to a metal surface, one can alter the electromagnetic boundary condition of the metal surface and, hence, its surface impedance, thereby changing its surface wave properties.

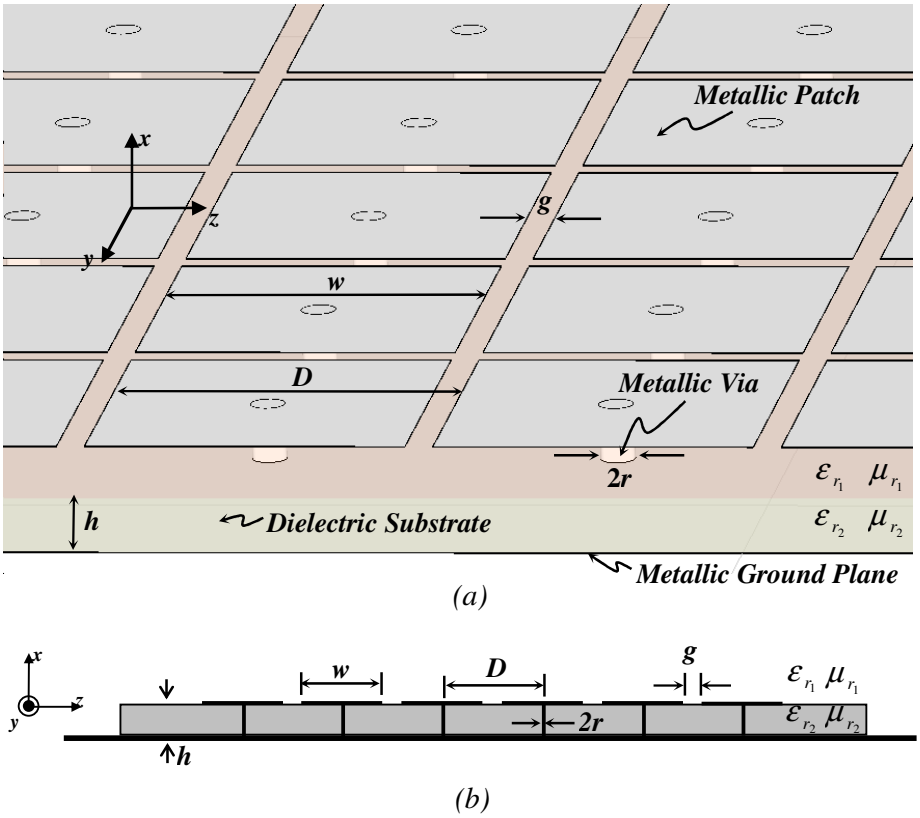

Figure 1 (a) Metallo-dielectric mushroom-like HIS-EBG surface; (b) Cross-sectional view of the mushroom-like HIS-EBG structure (from [8]).

The surface impedance of the mushroom-like HIS-EBG structure can be represented by a parallel resonant LC circuit and is given as

$$Z_{\text{surface}} = \frac{j\omega L}{1-\omega^2 LC} \tag{1}$$

where $\omega = 2\pi f$ and f define the angular frequency and frequency of the wave respectively. The equivalent sheet inductance, L, and the equivalent sheet capacitance, C, are given as follows:

$$L = \frac{\eta_s}{\omega}\tan(\beta h) \tag{2}$$

$$C = \frac{w\varepsilon_0\left(\varepsilon_{r_1} + \varepsilon_{r_2}\right)}{\pi}\cosh^{-1}\left(\frac{D}{g}\right) \tag{3}$$

where $\eta_s = \sqrt{\mu_0\mu_{r_2}/\varepsilon_0\varepsilon_{r_2}}$ and $\beta = \omega\sqrt{\mu_0\mu_{r_2}\varepsilon_0\varepsilon_{r_2}}$ define respectively the intrinsic wave impedance and the propagation constant. ε_0 and μ_0 are the permittivity and permeability of free space. The resonance frequency and the half-power bandwidth of the HIS-EBG structure are calculated as follows:

$$f_{\text{resonance}} = \frac{1}{2\pi\sqrt{LC}} \tag{4}$$

$$BW = \frac{Z_0}{\eta_0} \tag{5}$$

where $Z_0 = \sqrt{L/C}$ and $\eta_0 = \sqrt{\mu_0/\varepsilon_0} \approx 377\,\Omega$ are, respectively, the characteristic impedance of the surface and impedance of free space. The HIS-EBG supports TM surface waves at low frequencies and TE surface waves at high frequencies. Between these two bands near the resonance frequency, the imaginary part of the surface impedance of the HIS-EBG structure becomes very large, where both TE and TM surface waves are suppressed (i.e. the surface does not support bound surface waves), resulting in an electromagnetic surface wave band gap. It is noted that the half-power bandwidth, *BW*, over which the phase of the reflection coefficient falls from $+\pi/2$ to $-\pi/2$, and image currents are more in phase than out of phase, often coincides with the surface wave band gap.

From Eq. (4), increasing either the inductance or the capacitance can lower the resonance frequency and hence results in a compact size HIS-EBG design. In general, the HIS-EBG substrate thickness, *h*, is much less than the free space wavelength, λ_0, at the resonant frequency of the HIS structure, then from Eq. (2), the sheet inductance depends on the thickness of the substrate and the permeability of the substrate. Since at microwave frequencies, low-loss and high-permeability materials do not exist the inductance is fixed by the thickness. While increasing the substrate thickness increases the operational bandwidth, a trade-off must be made with the increased excitation of surface waves. On the other hand, without introducing lossy high-permeability material for a given thickness, an alternative way to lower the resonance frequency is to use capacitive loading. However, by using capacitive loading the structure will suffer from a reduction in bandwidth. Hence, a compromise must be made between inductive and capacitive loading for compact size HIS-EBG designs.

To understand the effect that each of the geometrical and material parameters has on the resonant frequency and on the bandwidth of the mushroom-like HIS-EBG structure, a parametric study is presented here where each of these parameters is varied separately in turn with other parameters retaining their original value, while keeping the period of the structure, *D*, constant. A broadband HIS structure suggested in [9], for application in aircraft High Intensity Radiated Fields (HIRF) protection, is chosen as the starting point for the parametric study where the period of the structure, *D*, is 12 mm and the HIS structure has the following parameters: the patch width, $w = 8$ mm, the gap width, $g = 4$ mm, the substrate thickness, $h = 12$ mm, the substrate permittivity, $\varepsilon_{r_2} = 1.05$. Figure 2 shows the resulting $f_{\text{resonance}}$ and *BW* for varying patch width, gap width, substrate thickness, and substrate permittivity. It is observed that when the patch width and/or substrate permittivity increase, both the resonant frequency and the bandwidth of the mushroom-like HIS-EBG structure decrease; when the gap width increases, both the resonant frequency and the bandwidth of the structure increase; and when the substrate thickness increases, the resonant frequency decreases and the bandwidth increases.

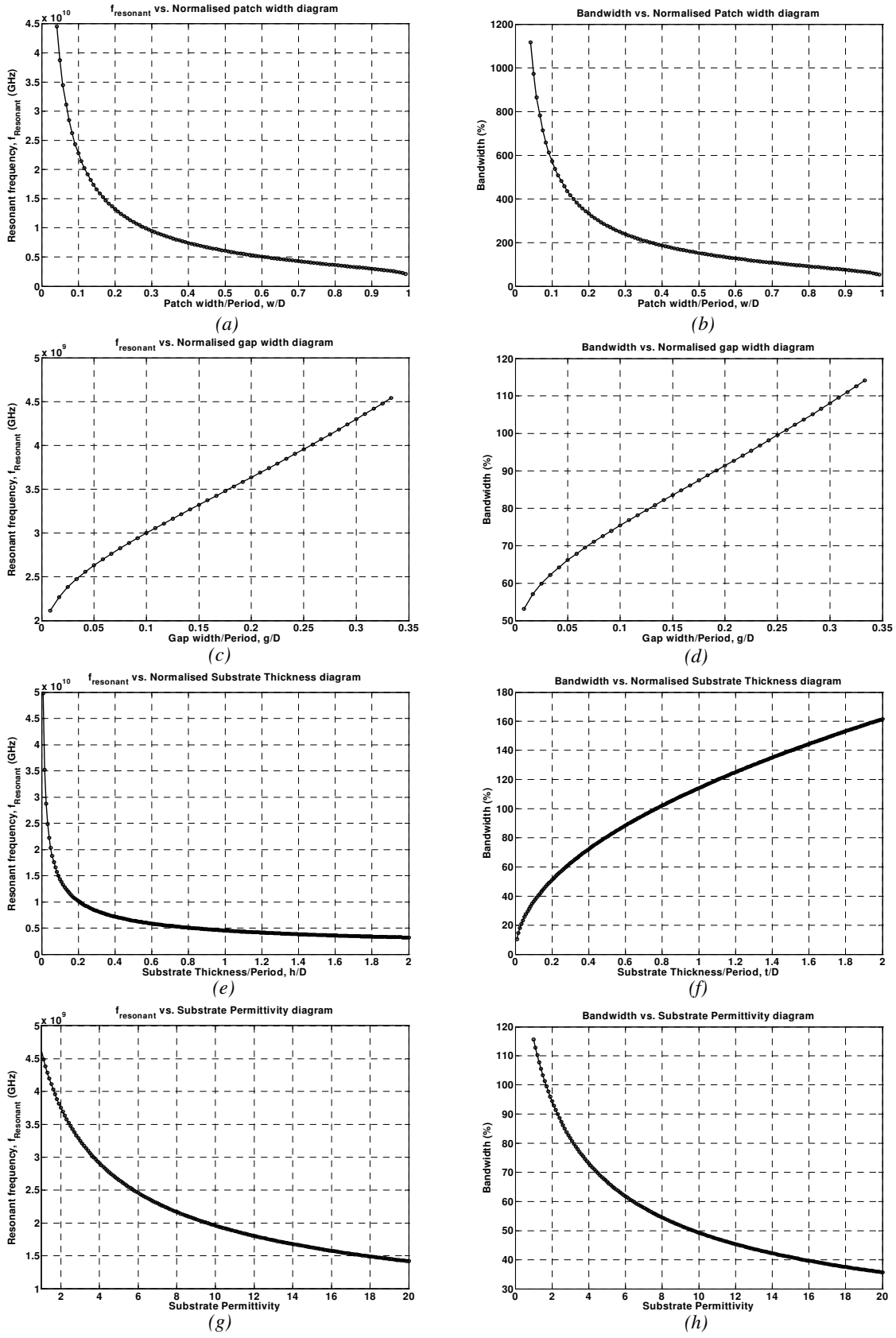

Figure 2 The resulting $f_{\text{resonance}}$ and BW for varying patch width (a & b), gap width (c & d), substrate thickness (e & f), and substrate permittivity (g & h).

An equivalent transmission line model for surface wave propagation

This section presents a novel approach to obtaining an equivalent transmission line circuit model for surface wave propagation of the varactor based tunable mushroom-like HIS-EBG where a top plate is introduced in parallel to the ground plane. As depicted in Figure 3, the electronically tunable HIS-EBG consisting of metallic square patches can be achieved by connecting adjacent patches with varactor diodes, thus altering the capacitance between them and hence the surface's resonance frequency. The varactor diode is assumed to have a junction capacitance, a series resistance, a package capacitance and a parasitic inductance [10].

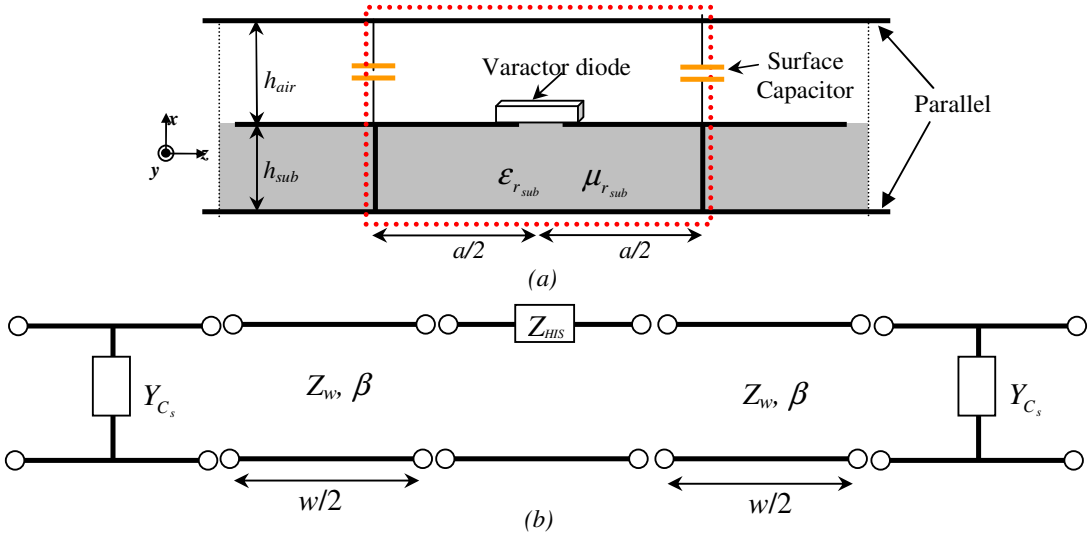

Figure 3 Unit cell of the varactor tunable mushroom-like HIS structure: (a) Lateral view, (b) equivalent two-port transmission line model.

The impedance of the varactor tunable HIS-EBG structure, Z_{HIS}, is given as follows:

$$Z_{HIS} = \frac{j\omega L_{HIS} - \omega^2 L_{HIS} R_{HIS} C_{HIS}}{1 - \omega^2 L_{HIS} C_{HIS} + j\omega R_{HIS} C_{HIS}} \tag{6}$$

where the resistance, capacitance and inductance of the tunable HIS-EBG structure, are:

$$R_{HIS} = \frac{1 + \omega^2 r_{pat}{}^2 C_{pat}{}^2}{\omega^2 C_{pat}{}^2 r_{pat}} \tag{7}$$

$$C_{HIS} = \frac{C_{pat}}{1 + \omega^2 r_{pat}{}^2 C_{pat}{}^2} \tag{8}$$

$$L_{HIS} = L_{pat} \tag{9}$$

The parameters r_{pat}, C_{pat}, L_{pat} are respectively the varactor dependent patch array series resistance, the geometry dependent patch array capacitance and the geometry dependent patch array inductance. It is noted that C_{pat} here is a sum of the geometry dependent fringing field capacitance and the varactor diode effective capacitance. From Fig. 3, the parameters β, Z_w and Y_w are the phase constant of the transmission line, the impedance and admittance of the propagating wave in an unloaded transmission line, respectively [11]. We define the five two-port circuit sections in Fig. 3(b) from the left to the right as increment block number from B1 to B5. The corresponding ABCD parameters of the three-cascaded two-port circuits, the first and the fifth two-port circuits are given as follows:

$$\begin{bmatrix} A & B \\ C & D \end{bmatrix}_{\text{B2–B4}} = \begin{bmatrix} \cos(\beta a) + j\frac{Y_w Z_{HIS}}{2}\sin(\beta a) & jZ_w\left(\sin(\beta a) - j\frac{Y_w Z_{HIS}}{2}\cos(\beta a) - j\frac{Y_w Z_{HIS}}{2}\right) \\ jY_w\left(\sin(\beta a) - j\frac{Y_w Z_{HIS}}{2}\cos(\beta a) + j\frac{Y_w Z_{HIS}}{2}\right) & \cos(\beta a) + j\frac{Y_w Z_{HIS}}{2}\sin(\beta a) \end{bmatrix} \quad (10)$$

$$\begin{bmatrix} A & B \\ C & D \end{bmatrix}_{\text{B1}} = \begin{bmatrix} A & B \\ C & D \end{bmatrix}_{\text{B5}} = \begin{bmatrix} 1 & 0 \\ Y_{C_s} & 1 \end{bmatrix} \quad (11)$$

where Y_{C_s} is the admittance of the surface capacitance. By cascading a few unit cells, the propagation characteristics of the waves within the structure can be evaluated. The following show the corresponding S-parameters for the two-port network using the ABCD parameters:

$$S_{21} = \frac{2}{A_{\text{B1–B5}} + B_{\text{B1–B5}}Y_w + C_{\text{B1–B5}}Z_w + D_{\text{B1–B5}}} \quad (12)$$

$$S_{11} = \frac{A_{\text{B1–B5}} + B_{\text{B1–B5}}Y_w - C_{\text{B1–B5}}Z_w - D_{\text{B1–B5}}}{A_{\text{B1–B5}} + B_{\text{B1–B5}}Y_w + C_{\text{B1–B5}}Z_w + D_{\text{B1–B5}}} \quad (13)$$

Based on the structure in [9], Fig. 4 shows the analytical results for the characterisation of surface wave propagation on the tunable mushroom-like HIS-EBG structure for number of period, $N = 10$. From the results, one observes that when the voltage across the varactors increases, the capacitance decreases and the resonance frequency increases.

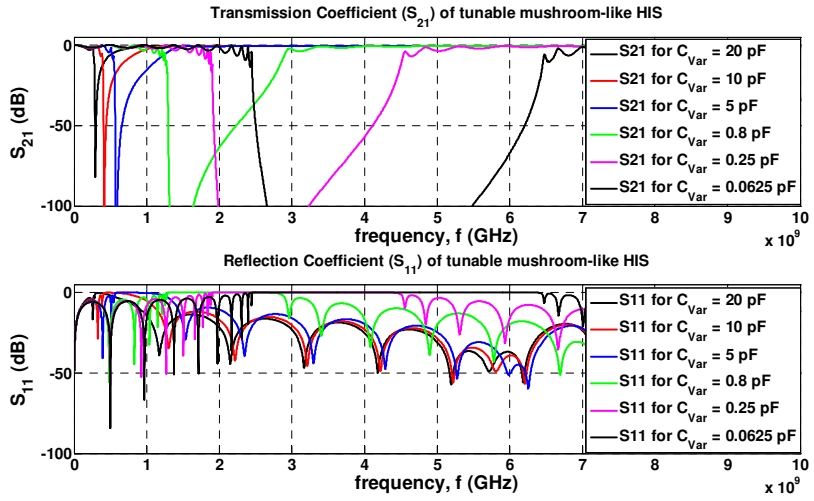

Figure 4 Analytical results for characterisation of surface wave propagation on the varactor tunable mushroom-like HIS structure [9] with the number of period, $N = 10$: (a) Magnitude of transmission loss, S_{21}, (b) Magnitude of return loss, S_{11}.

Applications for antenna engineering

The underlying interest in HIS-EBG metamaterials is the potential to tailor and manipulate their electromagnetic properties for a variety of antenna applications. With the two useful electromagnetic properties of HIS-EBG structures – in-phase reflection [12, 13] and surface wave suppression [14, 15], they have attracted increasing interest in the electromagnetic and antenna community. A useful list of EBG applications for antenna engineering has been given in [6]. In this section, the two useful electromagnetic properties of the HIS-EBG structures for applications to antenna engineering are discussed where the example results are presented for a wideband mushroom-like HIS EBG design [9], which has a resonant frequency of about 4.54 GHz. The design parameters are: $\varepsilon_{r_2} = 1.05$, $h = 0.18\lambda_{4.54\text{GHz}}$, $r = 0.0045\lambda_{4.54\text{GHz}}$, $w = 0.12\lambda_{4.54\text{GHz}}$,

$D = 0.18\lambda_{4.54\text{GHz}}$, and $g = 0.06\lambda_{4.54\text{GHz}}$, where $\lambda_{4.54\text{GHz}} = 66.08\,\text{mm}$ is the free space wavelength at the resonance frequency.

For antennas that use a flat metal sheet as reflector or ground plane a quarter-wavelength space between the radiating element and the ground plane is required to avoid poor radiation efficiency caused by the cancellation of the image currents with the currents in the antenna. This is illustrated in Figure 5(a). Although this idea can solve the problem, a minimum separation thickness of one-quarter-wavelength is required which is a crucial issue when limited space is available. In the frequency range where the surface impedance is very high, the tangential magnetic field is small, even with a large electric field. Hence with the use of a HIS-EBG structure, the problem above can be solved without the quarter-wavelength space, i.e. if the HIS-EBG substrate is applied the antennas can be placed as close as possible to the ground plane. The HIS-EBG substrate reflects all the power just like a metal sheet but its image current at the ground are in phase rather that out of phase with the antenna current. This is illustrated in Figure 5(b). For a normally incident wave, the reflection phase of the surface is given as

$$\Phi = \text{Im}\left[\ln\left(\frac{Z_{\text{Surface}} - \eta_0}{Z_{\text{Surface}} + \eta_0}\right)\right] \tag{14}$$

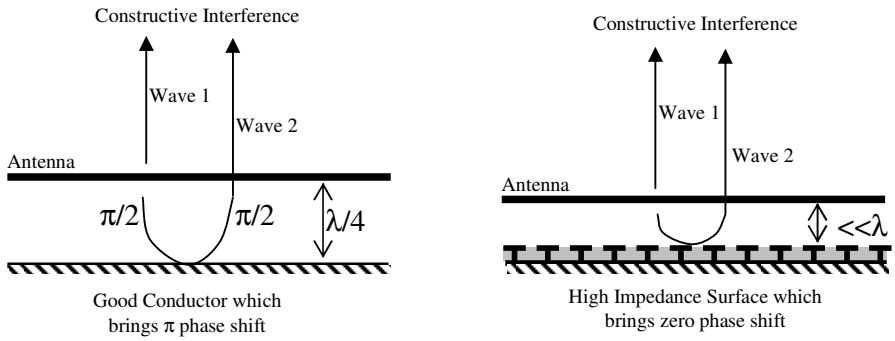

Figure 5 Reflection caused by various ground planes [7]: (a) An antenna separated by quarter wavelength from a flat metallic ground plane; (b) An antenna separated by a distance that is much less than the operating wavelength from a high-impedance ground plane.

The reflection phase of a HIS-EBG structure is a function of frequency as the surface impedance is frequency dependent. It is zero at the resonance frequency and it varies continuously from π to $-\pi$ as frequency increases. The reflection phase curve of a HIS-EBG surface crosses through $\pi/2$ and $-\pi/2$ near the edges of the surface wave band gap. This provides a useful reference to identify its operation band for antenna applications. Figure 6 shows the reflection phase curve of the wideband mushroom-like HIS-EBG design [9].

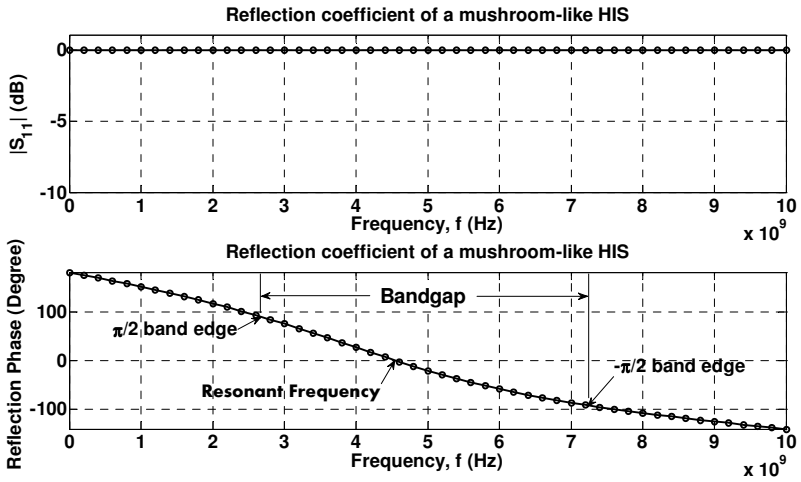

Figure 6 Reflection coefficient of the mushroom-like HIS EBG structure [9].

To study the bandgaps for surface wave propagation of a HIS-EBG structure, the dispersion relation for surface waves in the context of the effective surface impedance model needs to be determined, either by solving an eigenvalue equation or by performing a full wave simulation. Figure 7 shows the illustrative diagrams for TM and TE surface wave propagation on a mushroom-like HIS structure. Based on the effective surface impedance model in Eq. (1), the wavenumber, *k*, for TM and TE waves are given as follows:

$$k_{\mathrm{TM}}{}^2 = \frac{\omega}{c}\sqrt{1-\frac{Z_{\mathrm{surface}}{}^2}{\eta_0{}^2}} \tag{15}$$

$$k_{\mathrm{TE}}{}^2 = \frac{\omega}{c}\sqrt{1-\frac{\eta_0{}^2}{Z_{\mathrm{surface}}{}^2}} \tag{16}$$

where $c = 1/\sqrt{\mu_0\varepsilon_0}$ defines the speed of light. However, it is noted that there is no Brillouin zone boundary in the effective surface impedance limit, and the TM dispersion curve approaches the resonance frequency asymptotically. Thus, the effective surface impedance model does not predict the bandgap itself.

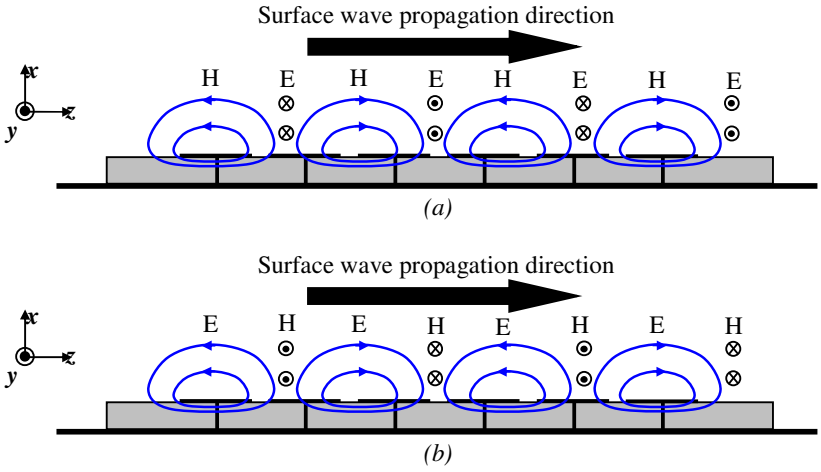

Figure 7 Surface wave propagation on mushroom-like HIS structure: (a) TM surface wave; (b) TE surface wave.

To obtain an accurate dispersion diagram and hence the electromagnetic bandgaps of the HIS-EBG structure, one can use commercially available numerical electromagnetic full wave simulator packages such as Vector Field Concerto [16], CST Microwave Studio [17], etc. In this work, CST Microwave Studio was used for the full wave simulations. Figure 8 shows the dispersion diagram of the lossless wideband mushroom-like HIS-EBG design [9] along the triangular path Γ–X–M–Γ relevant to the Brillouin zone. The circle solid plots in Fig. 8 are the solutions to their corresponding eigenvalue equations in which no solutions at given frequencies mean no wave propagation. The coloured area in Fig. 8 shows a complete bandgap in which no wave propagates in any directions.

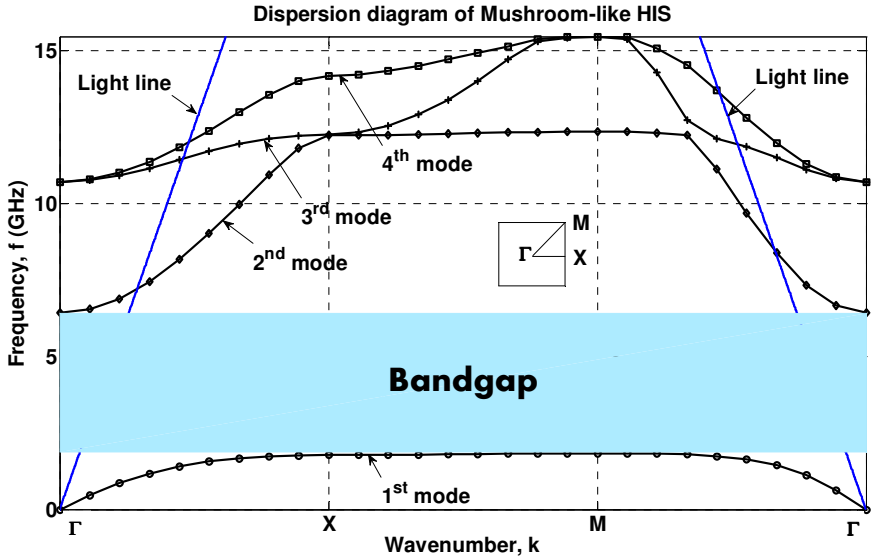

Figure 8 Dispersion diagram for surface wave propagation on the mushroom-like HIS structure [9]. The blue curves indicate the wave propagation in the air (i.e. light line) and coloured area shows the band gap of the corresponding HIS-EBG structure. Note that Γ, X, and M in the Brillouin zone represent the high symmetry points in the spectral domain, which correspond to ($k_x = k_y = 0$), ($k_x = \pi/a, k_y = 0$), and ($k_x = k_y = \pi/a$), respectively. The parameters a, k_x, k_y are the periodic interval of the unit cell, the wavenumber in the x-direction, and the wavenumber in the y-direction.

Conclusion

Mushroom-like HIS-EBG structures exhibit high surface impedances for both TE and TM polarisations and can suppress and enhance the wave propagation at certain frequency ranges. When a plane wave illuminates the HIS surface, an in-phase reflection coefficient is obtained resembling an artificial magnetic conductor. Furthermore, the surface wave band gap property of EBG helps to increase the antenna gain, minimise the backwards radiation, and reduce mutual coupling. Because of their desirable electromagnetic properties, they have been widely studied for potential applications in antenna engineering. In this work, a theoretical study of mushroom-like two-layer HIS-EBG structures, their design approaches and applications to antenna engineering has been conducted. A novel analytic equivalent transmission line circuit model for surface wave propagation of a tunable HIS structure have been presented where the effects of an additional top metal plate (e.g. patch antenna) for practical application are investigated. The model combines the transmission-line representation and the theory of periodic structures, which is a simple and fast approach for obtaining a first-step design of the HIS structure. The numerical simulations on the unit cell for obtaining dispersion diagram and reflection phase of the mushroom-like HIS-EBG structure were performed. A parametric study on the effects of patch width, gap width, substrate thickness and substrate permittivity were also presented. These results will be valuable for design and parameter selection.

Acknowledgements

This work was funded in part by the Physical Programme 2006 – 2009 of the National Measurement System (NMS) Policy Unit of the U.K. Department for Innovation, Universities and Skills (DIUS) and the Technology Strategy Board (TSB) Advanced Materials for Ubiquitous Leading-Edge Electromagnetic Technologies (AMULET) collaborative project.

References

[1] A. Scherer, *et al.*, *IEEE Trans. on Microwave Theory Tech., Special Issues on Electromagnetic Crystal Structures, Designs, Synthesis, and Applications,* vol. 47, Nov. 1999.

[2] N. Engheta and R. W. Z. (editors), *Metamaterials – Physics and Engineering Explorations*: Wiley InterScience, 2006.

[3] A. Aminian, *et al.*, "In-phase reflection and EM wave suppression characteristics of electromagnetic band gap ground planes," presented at the IEEE APS Int. Symp. Dig., Jun. 2003.

[4] T. H. Loh and C. Mias, "Photonic bandgap surfaces with interdigitated corrugations," *IEE Electron. Lett.,* vol. 40, pp. pp. 1123 - 1125, Sep. 2004.

[5] Y. L. R. Lee, *et al.*, "Dipole and tripole metallodielectric photonic bandgap (MPBG) structures for microwave filter and antenna applications," *IEE Proc. Optoelectron.,* vol. 147, pp. pp. 395 – 400, 2000.

[6] F. Yang and Y. Rahmat-Samii, *Electromagnetic Band Gap Structures in Antenna Engineering*: Cambridge University Press, 2009.

[7] D. Sievenpiper, *et al.*, "High-impedance electromagnetic surfaces with a forbidden frequency band," *IEEE Trans. on Microwave Theory and Tech.,* vol. 47, pp. pp. 2059 – 2074, 1999.

[8] T. H. Loh, "High Impedance Surface Electromagnetic Band Gap Metamaterials," Advanced Materials for Ubiquitous Leading-Edge Electromagnetic Technologies (AMULET), under deliverable for WP 1220 for TSB collaborative project number TP/8/ADM/6/I/Q2084L, Mar. 2009.

[9] S. P. Rea, *et al.*, "Broadband high-impedance surface design for aircraft HIRF protection," *IEE Proceedings Microwaves, Antennas and Propagation,* vol. 153, pp. pp. 307 – 313, 2006.

[10] C. Mias and J. H. Yap, "A varactor-tunable high impedance surface with a resistive-lumped-element biasing grid," *IEEE Trans. on Antennas and Propagation,* vol. 55, pp. pp. 1955 – 1962, Jul. 2007.

[11] K. C. Gupta, *et al.*, *Microstrip lines and slotlines*. Norwood, MA: Artech House, 1996.

[12] M. Rahman and M. A. Stuchly, "Circularly polarized patch antenna with periodic structure," *IEE Proc. Microwaves, Antennas and Propagation,* vol. 149, pp. pp. 141 - 146, 2002.

[13] D. Qu, *et al.*, "Improving microstrip patch antenna performance using EBG substrates," *IEE Proc. Optoelectron.,* vol. 153, pp. pp. 558 - 563, 2006.

[14] F. Yang and Y. Rahmat-Samii, "Microstrip antennas integrated with electromagnetic band-gap (EBG) structures: a low mutual coupling design for array applications," *IEEE Trans. on Antennas and Propagation,* vol. 51, pp. pp. 2936 - 2946, 2003.

[15] K. Buell, *et al.*, "Metamaterial insulator enabled superdirective array," *IEEE Trans. on Antennas and Propagation,* vol. 55, pp. pp. 1074 - 1085, 2007.

[16] Vector Field Concerto. Available: http://www.cobham.com/about-cobham/aerospace-and-security/about-us/antenna-systems/kidlington.aspx

[17] CST Microwave Studio. Available: http://www.cst.com/